# Comparative Analysis of Decoupling Control Methods for Multiport-Isolated Bidirectional DC-DC Converter with Hydrogen Storage System Integration

Oyedotun E. Oyewole
*Electronic & Electrical Engineering*
*University of Strathclyde*
Glasgow, UK
oyedotun.oyewole@strath.ac.uk

Khaled H. Ahmed
*Electronic & Electrical Engineering*
*University of Strathclyde*
Glasgow, UK
khaled.ahmed@strath.ac.uk

***Abstract*— Hydrogen storage systems have garnered increasing interest over the years, owing to their positive environmental implications. The efficiency of such systems is closely related to the efficiency of their power electronics interface. Multiport-isolated bidirectional DC-DC converters offer several advantages over other converters, including lower power density, bidirectional functionality, reduced component counts, soft switching ability, and a reduced number of conversion stages. However, these converters suffer from the cross-coupling effect of the control variables with the power dissipated at each port, which significantly impacts the system's response to step changes and limits its reliability. This paper presents a comprehensive comparison of three different decoupling control methods for multiport-isolated DC-DC converter to establish the effects of cross-coupling. Simplified, Inverted, and GH matrix-decoupling control methods are implemented. The simulation results show that better system response is achieved using decoupling control methods. The GH matrix decoupling method provides superior performance in terms of reduced peak power deviation and settling time when cross-coupling occurs.**

***Keywords*— *Decoupling control, Hydrogen Storage System, PI Controller, cross-coupling, Triple Active Bridge.***

## I. INTRODUCTION

A hydrogen energy storage system is a technology that uses hydrogen as a medium for storing energy, which can be used to generate electricity or for other power applications. Hydrogen is a clean and renewable energy source that can be produced from water using electrolyzers (EL), which require electricity. In a hydrogen energy storage system, excess electricity generated from Distributed Energy (DE) sources and/or Renewable Energy sources (RE) is used to split water into hydrogen and oxygen. The hydrogen is then compressed and stored in tanks or containers until required. The stored hydrogen can be used to generate electricity using Fuel Cells (FC) to satisfy immediate and long-term energy demands. It is also used in domestic heating/commercial heating, vehicular fuel, and domestic cooking [1]. Three major stages are involved in hydrogen technology: hydrogen production, hydrogen storage, and hydrogen re-electrification, as explained in [1, 2]. Fig. 1 shows the concept of the production and utilization of hydrogen for electricity generation and its interface with existing power systems with the aid of power electronic converters. Converters are very important in increasing/decreasing voltage and producing the required voltage conditioning, as the EL and FC exhibit nonlinear behaviour [3]. In the literature, several studies have been reported about converters used for FCs, but little has been reported regarding converters for EL applications [3-5].

The EL and FC have specific requirements that must be satisfied by the candidate topologies of the interface system to ensure continued production, storage, and use of hydrogen. For example, candidate topologies for this application must have a high flexible voltage conversion ratio, low current ripple, relatively high current delivery, high efficiency, high power density, high fault tolerance, and high tuning performance [3-5]. These topologies can either be isolated topologies or non–isolated topologies, which are differentiated by galvanic isolation between the source and sink for safety reasons [4].

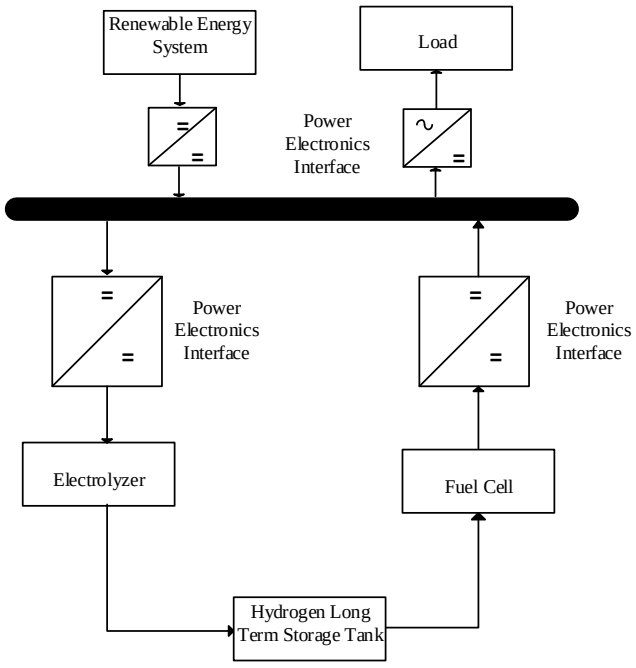


Fig. 1: Hydrogen energy storage system with conventional power electronics interface.

Several topologies have been highlighted in the literature to provide good performance for specific application requirements. However, designing a hydrogen storage system with multiple power conversion needs that also meet these requirements poses some problems and limitations [6-8] [9, 10]. In such a system, the converters cannot operate independently of each other, resulting in bulkiness and increased costs. The multiple power transfer between ports

will also increase the circulating current, negatively impacting the storage elements' life and reducing the efficiency of the converter.

Multiport DC-DC converters are developed to reduce the complexity of various interconnected interfaces and integrate multiple energy sources and energy storage devices using a single interface [9, 11]. They have the benefits of a reduced number of separate converters, improved power density, improved fault tolerance, reduced cost, ease of control, and a smaller component count.

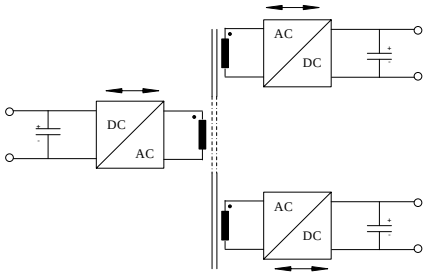


Fig. 2: A 1:2 DC-DC multiport-isolated converter.

The isolated topology of the multiport converter, a triple active bridge converter (TAB), as depicted in Fig. 2, has advantages over non-isolated topologies, such as galvanic isolation, relatively low power density, ease of control, and cascading[12]. Multiport-isolated DC-DC converters can be derived from several combinations of FC/EL topologies. However, despite the many interface topologies developed for FC, supercapacitors, electrochemical batteries, mechanical energy storage (wind energy), and solar cell applications, there are few reports on hydrogen storage systems.

Despite the advantages of multiport topology, there are trade-offs. Depending on the application and control use, the dynamic response of the converter is a subject of active research [13, 14]. When there is a mismatch of certain parameters (for example, load mismatch or impedance mismatch), currents settle between the legs of the converter, resulting in an unwanted circulating current, which incurs losses in the system and an efficiency drop [15-21].

In addition, a high level of coupling effect exists between the phase shifts and the power delivered at each port, which makes it difficult to manage the currents and voltages at each of the ports because of the use of the multi-winding transformer. Essentially, the converter behaves like a Multiple-Input Multiple-Output (MIMO) system with a coupled controlled loop. A multiport converter with inherent decoupling ability was developed in [22, 23] with the argument that a low or zero external inductive element at the source and a higher external inductive element at other ports can inherently cancel out the effect of cross-coupling on each port. This is beneficial as no external components are needed to achieve this; however, the calculation seems complex, and it is not proven for a larger system as there are various possible values of the external inductor that could be selected. In [24], the coupling effect was reduced by identifying the coupled element in the nonlinear dynamic equation of the converter and by extracting the element from the principle given by [25]. The extracted coupled element is then used in the power equation of each port to derive the decoupled power at each sinking port. The use of different bandwidths for single-input single-output and implementing the loop with the highest bandwidth to determine the direction of phase shifts during transients helps decouple the system, as discussed in [26]. A technique to operate two active bridges like a Dual Active Bridge (DAB) while the third is controlled to act like a diode rectifier has been proposed in [27]. This essentially limits the influence of the changes in one port on the other. A system transfer matrix was developed in [28-30] to observe the effect of coupling between ports, and a decoupling matrix was formulated to limit the coupling effect of the transfer matrix. However, no detailed research has been conducted to compare the performances of these decoupling techniques.

In this paper, a comparative study of three decoupling methods are carried out to evaluate their performance and pave the way for further research and analysis.

The remainder of this paper is organised as follows. The topology, equivalent circuit, and power flow of a multiport converter (triple port) are discussed in Section II. Section III explains the cross-coupling effects and decoupling control methods. Section IV presents the simulation results and discussion.

## II. TOPOLOGY

Multiport-isolated DC-DC converters are derived from the principles of a DAB with the addition of more legs to either side of the transformer. This can result in symmetric or asymmetric configurations. A 1:2 asymmetric triple-active bridge converter configuration is analysed in the following section.

### *A. Equivalent Circuit*

The topology is shown in Fig. 3 and is made up of full-bridge converters. The primary port is labelled as the main distributed energy source (DE) (port 1), the secondary port is labelled as the FC port (port 2), and the tertiary port is labelled as the EL port (port 3). DE and FC are represented as a voltage source, and EL is represented as a resistive load for simplicity of analysis. These ports are connected through a three-winding transformer. Negative power depicts power dissipation from a port, and positive power depicts the power absorbed from the corresponding port.

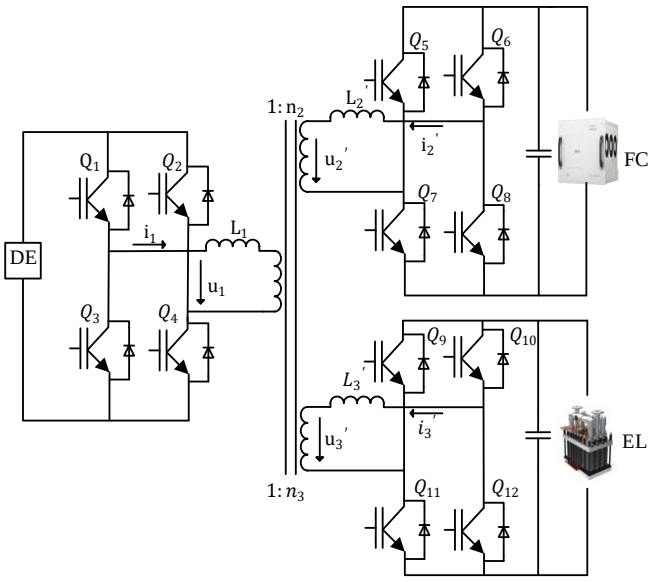


Fig. 3: Multiport-isolated bidirectional dc-dc converter for hydrogen storage systems.

The equivalent circuit of the converter is illustrated in Fig.

4, as explained in [31-33]. In Fig. 4, $L_m$ is the magnetising inductance, and the two ideal transformers are $T_1$ and $T_2$ with turn ratios of $1:n_2$ and $1:n_3$. Power transfer is influenced by the leakage inductance of the high-frequency transformer, which is determined by the phase shift of each full-bridge control signal. In this topology, external inductances are used because the leakage inductance of the transformer may be low. $L_1$ is the primary bridge leakage inductance, $L'_2$ is the secondary leakage inductance and $L'_3$ is the tertiary leakage inductance, all referred to the primary side [34, 35]. The equivalent circuit of the system in the T model is presented in Fig. 4b.

The parameters are defined as follows: The output signals of each bridge's square-wave voltage are presented as $u'_2$, $u'_3$ with a duty cycle of 0.5. The external leakage inductances, currents, and voltages all referred to the primary side (DE port) are symbolised as $L'_2, i'_2, u'_2, V'_2$ and for the tertiary bridge as $L'_3$ , $i'_3$ , $u'_3$, $V'_3$. Therefore, $u_2 = \frac{u'_2}{n_2}$ , $V_2 = \frac{V'_2}{n_2}$ , $L_2 = \frac{L'_2}{n_2^2}$ , $i_2 = i'_2 n^2$ and $u_3 = \frac{u'_3}{n_3}$ , $V_3 = \frac{V'_3}{n_3}$ , $L_3 = \frac{L'_3}{n_3^2}$ , $i_3 = i'_3 n^2$. $V'_3$ and $V'_2$ are the DC voltage values of the EL and FC ports, respectively.

To facilitate the power flow analysis, it is necessary to calculate the equivalent inductances between each port. This requires converting the T model to the pi model, which allows transmission power analysis by superimposing the power transfer of each adjacent port [10]. Fig. 4c illustrates this approach. The leakage inductances of the pi model $L_{12}$ , $L_{13}$, $L_{23}$ , as seen in [36] can be expressed as:

$$L_{12} = \frac{L_1L_2 + L_2L_3 + L_1L_3}{L_3} \quad (1)$$

$$L_{13} = \frac{L_1L_2 + L_2L_3 + L_1L_3}{L_2} \quad (2)$$

$$L_{23} = \frac{L_1L_2 + L_2L_3 + L_1L_3}{L_1} \quad (3)$$

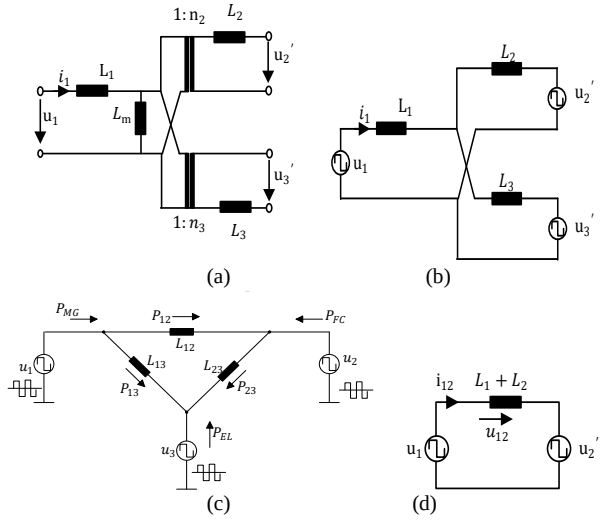


Fig. 4: Equivalent circuit of the converter (a) equivalent circuit of three port isolated system (b) T network of the system (c) pi network of the system (d) equivalent circuit when one port is zero.

### *B. Power Flow of the Converter*

The output voltages of each full bridge are represented by square-wave voltage sources with a duty cycle of 50 % [32]. This is created by alternately driving the gate signals of switches $Q_1$and $Q_4$ , $Q_2$ and $Q_3$ of the reference bridge. Correspondingly, the gate signals of $Q_5$ and $Q_8$ , $Q_7$ and $Q_6$ and the gate signals of $Q_9$ and $Q_{12}$ , $Q_{11}$ and $Q_{10}$ of both the FC and EL bridges are alternately driven. The phase shift of the control signals $u_1$ and $u'_2$ is denoted as $\varphi_2$ and the phase shift between $u_1$ and $u'_3$ is denoted as $\varphi_3$. This is typically called the single-phase shift control in a dual active bridge extended to the multiport active bridge [34, 37, 38].

The phase shifts can either be positive or negative depending on the lagging or leading attributes of the corresponding bridge square-wave voltages. For instance, if $u_1$ is leading $u_2$, then $\varphi_2$ is positive similarly when $u_1$ is leading $u_3$, $\varphi_3$ is positive and vice versa. The maximum power is delivered at $\frac{\pi}{2}$, therefore the range of the phase shifts must be limited to between $-\pi$ and $\pi$.

As calculated in [32], the three-port DC-DC converter can be simplified into a simple two-port converter when the third port is left open, as shown in Fig. 4d. Therefore, the power flow between the two ports is given as:

$$P_{12} = \frac{\varphi_2(\pi-\varphi_2)V_1V_2}{2\pi^2 f_s L_{12}} \quad (4)$$

where, $V_1$ and $V_2$ are the magnitudes of the $u_1$ and $u_2$, and $f_s$ is the switching frequency.

From (4), the direction and magnitude of the power flow are given by the phase shift angles between the two corresponding ports. For a hydrogen storage system, the following equation must be satisfied, $P_{DE} + P_{FC} + P_{EL} = 0$.

Six possible modes can be generated from the triple active bridge, however for this application three modes $\varphi_2 < 0$ and $\varphi_3 < 0$ and $\varphi_2 < \varphi_3$ is essential. The power in each port is given as (neglecting losses):

$$P_{DE} = -P_{12} - P_{13} \quad (5)$$

$$P_{FC} = P_{12} - P_{23} \quad (6)$$

$$P_{EL} = P_{13} + P_{23} \quad (7)$$

The following can be obtained for the TAB topology:

$$P_{DE} = \frac{\varphi_2(\varphi_2-\pi)V_1V_2L_3 + \varphi_3(\varphi_3-\pi)V_1V_3L_2}{2\pi^2 f_s(L_1L_2+L_2L_3+L_1L_3)} \quad (8)$$

$$P_{FC} = \frac{\varphi_2(\varphi_2-\pi)V_1V_2L_3 + (\varphi_3-\varphi_2)(\varphi_2-\varphi_3-\pi)V_2V_3L_1}{2\pi^2 f_s(L_1L_2+L_2L_3+L_1L_3)} \quad (9)$$

$$P_{EL} = \frac{\varphi_3(\pi-\varphi_3)V_1V_3L_2 + (\varphi_3-\varphi_2)(\pi-\varphi_2+\varphi_3)V_2V_3L_1}{2\pi^2 f_s(L_1L_2+L_2L_3+L_1L_3)} \quad (10)$$

It can be seen clearly from the equation that a nonlinear relationship exists between the power of each port and the phase shifts. The phase shifts also exhibit a coupling relationship with each other.

## III. DECOUPLING AND CONTROL

As seen in equations (8-10), the cross-coupling effect of the phase shifts (which are the control variables) on the power equation needs to be eliminated to allow for easy control of the system. The following section explains this concept and provides insights into the employed control system.

The control objective is to derive a feedback control system to regulate power in the output ports. However, the power equations of (8-10) are nonlinear with phase shift ratios $\varphi_2$ and $\varphi_3$.

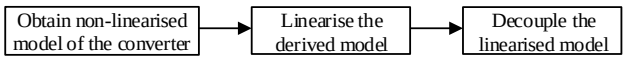


Fig. 5: Steps to decoupling.

Conventional generalised average modeling is difficult to use for multiport-isolated DC-DC converters because the integral value over one switching cycle is always zero, therefore, the dynamic properties of the external inductors are neglected [28, 30]. Following the steps shown in Fig. 5, the obtained nonlinear model must be linearized. To derive the linearized model from (9-10) without considering the different magnitudes of the phase shifts, a sinusoidal approximation, as seen in (11)–(12), is applied:

$$\varphi = (\pi - |\varphi|) \approx X \sin\varphi \tag{11}$$

where X can be derived from the Fourier coefficient:

$$X = \frac{1}{\pi}\int_{-\pi}^{\pi} \varphi(\pi - |\varphi|) \sin\varphi \, d\varphi = \frac{8}{\pi} \tag{12}$$

Expressing the controlled objectives in equations (9-10) gives rise to a quadratic equation as seen in (13-14).

$$I_{\mathrm{fc}} = \frac{4(\mathrm{V_1L_3}sin\varphi_2 + \mathrm{V_3L_1}sin(\varphi_2-\varphi_3)}{\pi^3 \mathrm{f_s} A} \tag{13}$$

$$I_{el} = \frac{4(\mathrm{V_1L_2}sin\varphi_3 + \mathrm{V_2L_1}sin(\varphi_3-\varphi_2)}{\pi^3 \mathrm{f_s} A} \tag{14}$$

The converter has to be linearized based on a selected operating point of the phase shifts. There are four possible solutions of $\varphi_2$ and $\varphi_3$. According to [31], the operating point is the solution with the lowest phase shifts resulting in the lowest conduction and switching losses. The equation can be linearized with $\varphi_2$ *and* $\varphi_3$ approximations close to the origin. Using the Taylor series expansion truncated at the first-order term,

$$\mathrm{f}((\varphi_2,\varphi_3) = \mathrm{f}((\varphi_{2\mathrm{p}},\varphi_{3\mathrm{p}}) + \frac{\partial \mathrm{f}}{\partial \varphi_{2,}}\Big|_{\varphi_{2p},\varphi_{3p}} (\varphi_2 - \varphi_{2p}) + + \frac{\partial \mathrm{f}}{\partial \varphi_3}\Big|_{\varphi_{2p},\varphi_{3p}} (\varphi_{3p} - \varphi_{3p}) \tag{15}$$

$I_{fc}$ *and* $I_{el}$ can then be expressed as:

$$\begin{bmatrix} I_{\mathrm{fc}} \\ I_{\mathrm{el}} \end{bmatrix} = \begin{bmatrix} \frac{4(\mathrm{V_3L_1}+\mathrm{V_1L_3})}{\pi^3 \mathrm{f_s} A} & \frac{-4\mathrm{V_3L_1}}{\pi^3 \mathrm{f_s} A} \\ \frac{-4\mathrm{V_2L_1}}{\pi^3 \mathrm{f_s} A} & \frac{4(\mathrm{V_2L_1}+\mathrm{V_1L_2})}{\pi^3 \mathrm{f_s} A} \end{bmatrix} \begin{bmatrix} \varphi_2 \\ \varphi_3 \end{bmatrix} \tag{16}$$

with $A = \mathrm{L_1L_2} + \mathrm{L_2L_3} + \mathrm{L_1L_3}$.

Equation (16) shows the coupling effects between $I_{\mathrm{fc}}$ and $I_{\mathrm{el}}$. Therefore, the plant transfer matrix G can be represented as:

$$\begin{bmatrix} I_2 \\ I_3 \end{bmatrix} = G \begin{bmatrix} \varphi_2 \\ \varphi_3 \end{bmatrix} \tag{17}$$

Equation (16) forms a two-input, two-output model with plant transfer matrix G. The output currents interfered with each other. The process of eliminating the interference by systematically choosing a matrix that will limit or cancel out the effect of this interference is the decoupling control. The chosen matrix is referred to as a decoupling matrix.

### *A. GH Matrix Decoupling*

In this method, the cross-coupling effect is eliminated by choosing a matrix that is the inverse of the plant transfer matrix. This method has no negative effect on ideal plant properties.

If we introduce an inverse of matrix G into (17), the diagonal input-output matrix is derived as in (18).

$$\begin{bmatrix} \varphi_2 \\ \varphi_3 \end{bmatrix} = H \begin{bmatrix} \varphi'_2 \\ \varphi'_3 \end{bmatrix} = G^{-1} \begin{bmatrix} \varphi'_2 \\ \varphi'_3 \end{bmatrix} \tag{18}$$

Where $H$ is the decoupling matrix (19) resulting in a fully decoupled equation (20).

$$H = \frac{1}{4K\mathrm{V_1}} \begin{bmatrix} \pi^3 \mathrm{f_s} A(\mathrm{V_1L_2} + \mathrm{V_2L_1}) & \pi^3 \mathrm{f_s} A \mathrm{V_3L_1} \\ \pi^3 \mathrm{f_s} A \mathrm{V_2L_1} & \pi^3 \mathrm{f_s} A(\mathrm{V_1L_3} + \mathrm{V_3L_1}) \end{bmatrix} \tag{19}$$

with $K = \mathrm{V_3L_1L_2} + \mathrm{V_1L_2L_3} + \mathrm{V_2L_1L_3}$.

$$M = \begin{vmatrix} \mathrm{G_{11}} & \mathrm{G_{12}} \\ \mathrm{G_{21}} & \mathrm{G_{22}} \end{vmatrix} \begin{vmatrix} \mathrm{H_{11}} & \mathrm{H_{12}} \\ \mathrm{H_{21}} & \mathrm{H_{22}} \end{vmatrix}$$

$$\begin{bmatrix} I_2 \\ I_3 \end{bmatrix} = \begin{bmatrix} \mathrm{M_{11}} & \mathrm{M_{12}} \\ \mathrm{M_{21}} & \mathrm{M_{22}} \end{bmatrix} \begin{bmatrix} \varphi'_2 \\ \varphi'_3 \end{bmatrix} \tag{20}$$

Consequently, the product of G and H results in a diagonal matrix M, which shows that the coupling between inputs 1 and 2 and vice versa is eliminated.

Although this is easy to implement, it is worth noting that sometimes, when dealing with dynamic equations, obtaining the inverse of the transfer function poses a problem. The inverse results in an unrealisable improper transfer function.

A block diagram of the fully decoupled system using the GH matrix decoupling method is shown in Fig. 6.

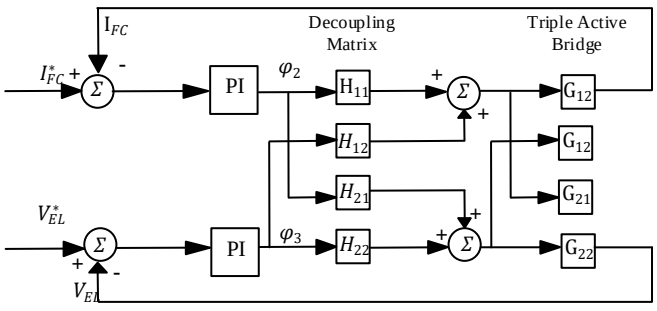


Fig. 6: GH decoupling methods schematics.

### *B. Simplified Decoupling Method*

In the simplified decoupling method, only two elements in the decoupling matrix must be generated compared to the four elements generated in the GH decoupling method. This sets two elements in the diagonal of the decoupling matrix to one, such that matrix $H$ is $[1\ \mathrm{H_{12}}; \mathrm{H_{21}}\ 1]$.

Therefore, in expression, relating matrix H in terms of the transfer matrix of the plant is given as in (21).

$$H = \begin{bmatrix} 1 & -\frac{\mathrm{G_{12}}}{G_{11}} \\ -\frac{\mathrm{G_{21}}}{G_{22}} & 1 \end{bmatrix} \tag{21}$$

Although simple to implement in practice, there are some summation elements in the decoupling matrix, which makes

tuning the controller difficult. A schematic of the simplified method is shown in Fig. 7.

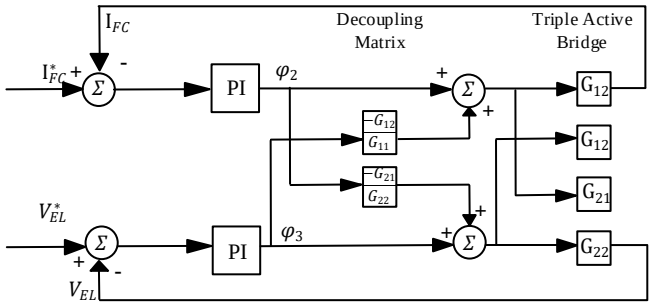


Fig. 7: Simplified decoupling method control schematics.

*C. Inverted Decoupling Method*

The inverted decoupling method is another method used to generate a decoupling matrix to eliminate cross-coupling effects. Here, $H_{12}$ and $H_{21}$ are set to one such that,

$$H_{12} = -\frac{G_{12}}{G_{11}} \quad (22)$$

and

$$H_{21} = -\frac{G_{21}}{G_{22}} \quad (23)$$

As stated in [39, 40], inverted decoupling has the same required compensation elements as simplified decoupling. However, as shown in Fig. 8, the direction of the flow through the decoupling elements and the position of the summation are reversed when compared to the simplified decoupling.

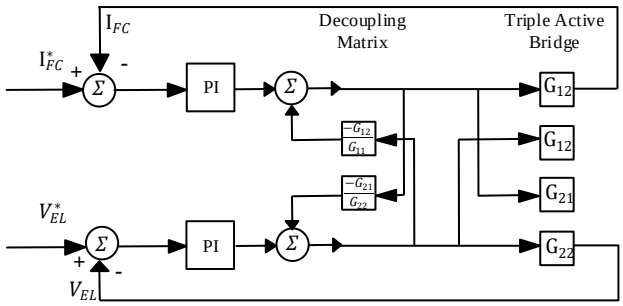


Fig. 8: Inverted decoupling methods control schematics.

It has a simple implementation and can always be configured such that its decoupling element is realisable. However, to achieve this, additional elements must be added to the system, which does not guarantee that the physical properties of the decoupling matrix will not be tampered with.

In general, the control scheme aims to regulate power flow in the circuit. The PI-based calculation of phase $\varphi_2$ is summarised as follows:

$$\varphi_2 = K_P(P_{FC} - P_{FC}^*) + \frac{K_I}{s}(P_{FC} - P_{FC}^*) \quad (24)$$

Where $K_P$ is the proportional gain and $K_I$ is the integral gain of the PI controller. The second PI used for voltage control follows the same principle as the EL, as it is for the FC. Thus, its equation is given as:

$$\varphi_3 = K_P(V_{EL} - V_{EL}^*) + \frac{K_I}{s}(V_{EL} - V_{EL}^*) \quad (25)$$

In these control schemes, the energy delivered by the DE is not controlled directly. It is allowed to freely sink or source the power difference between the EL and the FC. This is similar to a self-directed system that matches the EL voltage variations while maintaining a constant FC power. The control scheme without a decoupler is shown in Fig. 9.

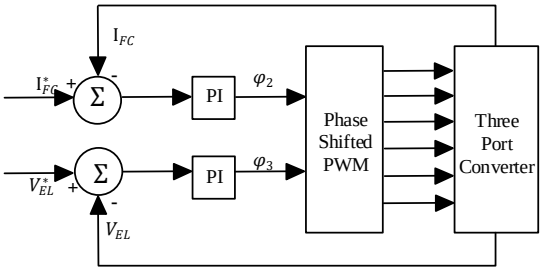


Fig. 9: Control scheme of the converter.

## IV. SIMULATION RESULTS

The designed topology is a 1 kW bi-directional triple active bridge DC-DC converter with circuit parameters given in Table 1 following [41] with little adjustments to the main parameters.

TABLE 1
CIRCUIT DESIGN PARAMETERS

| Description | Parameter |
|---|---|
| FC Voltage | 46 V |
| EL Voltage | 73 V |
| DE DC Voltage | 560 V |
| Leakage Inductance 1 | 0.75 mH |
| Leakage Inductance 2 | 1 µH |
| Leakage Inductance 3 | 24 µH |
| Switching frequency | 15 kHz |
| Transformer Turns Ratio ($n_1$) | 0.08 |
| Transformer Turns Ratio ($n_2$) | 0.13 |

The circuit in Fig. 3, is implemented in the MATLAB/SIMULINK software environment along with the PI control scheme shown in Fig. 6-9. The controller gains are tuned and selected, as listed in Table 2, for both the current and voltage loops. The components are all referred to the primary side. Fig. 10 shows the measured steady-state operation results of the square-wave voltages and inductor currents at each port. It can be seen that the shapes of $I_{de}$ and $I_{el}$ are trapezoidal following the same analogy as a DAB converter. However, the shape of the main supply port ($I_{fc}$) is not trapezoidal because it complements the trapezoidal-shaped currents of the other ports. The results also show that, as long as there is a unity conversion ratio, the converter experiences soft switching.

TABLE 2
SELECTED PROPORTIONAL AND INTEGRAL GAINS

| | Proportional Gain | Integral Gain |
|---|---|---|
| Without decoupler | 0.05 | 2000 |
| GH Matrix decoupler | 5 | 8000 |
| Simplified decoupler | 1 | 1200 |
| Inverted decoupler | 0.8 | 800 |

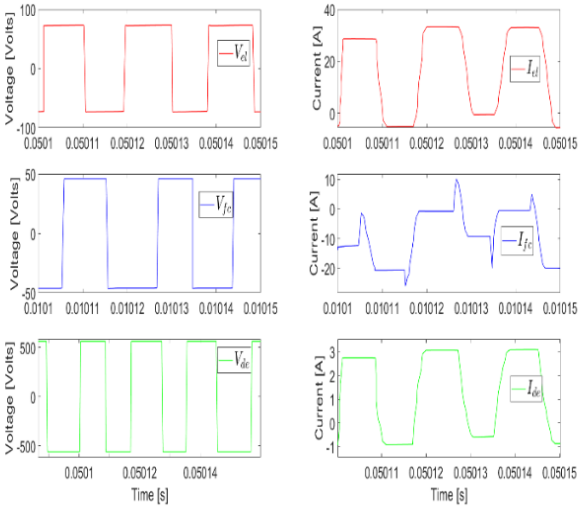


Fig. 10: Bridge voltages and inductor currents at steady state for unity conversion ratios.

The cross-coupling effect on the plant transfer matrix allows for the disturbance to be measured across a port when there is an intended or unintended change at the other port. Two scenarios are created to test the performance of the decoupling method. Three-step changes are introduced to the current control loop at specific times to create Scenario 1. There is a change in the control current from -5 A to -22 A, -22 A to -9 A, and -9 A to -4 A as shown in Fig. 12. In Scenario 2, an increase in the EL voltage from 10 V to 73 V is introduced, and a drop in the load demand is made from 72 V to 42 V and 42 V to 18 V. In each scenario, the peak power deviations and settling times are measured to ascertain the influence of the cross-coupling effect on each controlled port, as listed in Table 3. The lower the peak power deviation from the steady-state values at each control point, the better the decoupling performance.

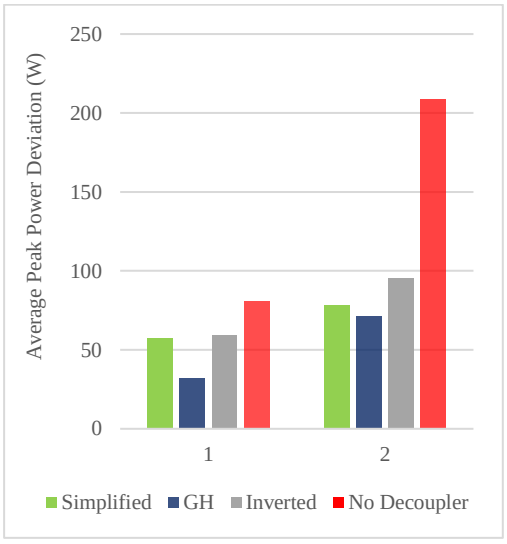


Fig. 11: Peak power deviation.

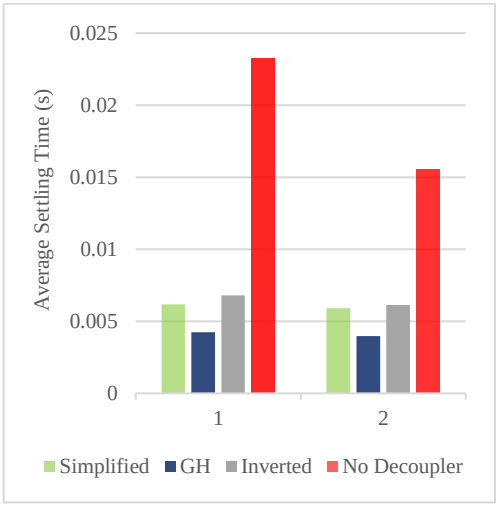


Fig. 12: Settling time.

TABLE 3
PEAK POWER DEVIATIONS AND SETTLING TIMES CONSIDERING DIFFERENT DECOUPLING METHODS

| | | Scenario 1 | | Scenario 2 | |
|---|---|---|---|---|---|
| Method | Time (s) | Power Deviation (W) | Settling Time (s) | Power Deviation (W) | Settling Time (s) |
| Simplified | 0.05 | 80 | 0.0066 | 124 | 0.0113 |
| | 0.1 | 64 | 0.0062 | 59 | 0.0034 |
| | 0.15 | 28 | 0.0057 | 52 | 0.0030 |
| GH | 0.05 | 45 | 0.0063 | 93 | 0.0070 |
| | 0.1 | 34 | 0.0039 | 64 | 0.0023 |
| | 0.15 | 16 | 0.0025 | 56 | 0.0026 |
| Inverted | 0.05 | 80 | 0.0068 | 156 | 0.0091 |
| | 0.1 | 68 | 0.0072 | 59 | 0.0048 |
| | 0.15 | 29 | 0.0064 | 71 | 0.0045 |
| No Decoupling | 0.05 | 136 | 0.0430 | 193 | 0.0172 |
| | 0.1 | 77 | 0.0137 | 276 | 0.0159 |
| | 0.15 | 29 | 0.0131 | 157 | 0.0135 |

It can be seen that with the implemented decoupling controller, the peak power deviations (either overshoot or undershoot) are limited in each control method compared to the converter without decoupling control. This shows that implementing decoupling control improves the dynamic performance of the system. System stability and adequate power balancing can also be achieved, as shown in Fig. 13-14. In each scenario, the DE port acts as a freewheeling port and is allowed to sink or source, thereby maintaining an adequate balancing of the system. With this, higher efficiency can be achieved while also protecting the lifespan of the EL and FC and preventing false triggering of protective devices sensitive to overshoot and undershoot voltages.

The average peak power deviation from the steady-state value and the average settling time for the three-step changes were calculated, as shown in Fig. 11-12. It can be seen that the GH matrix decoupling method has a reduced peak power deviation and a fast settling time.

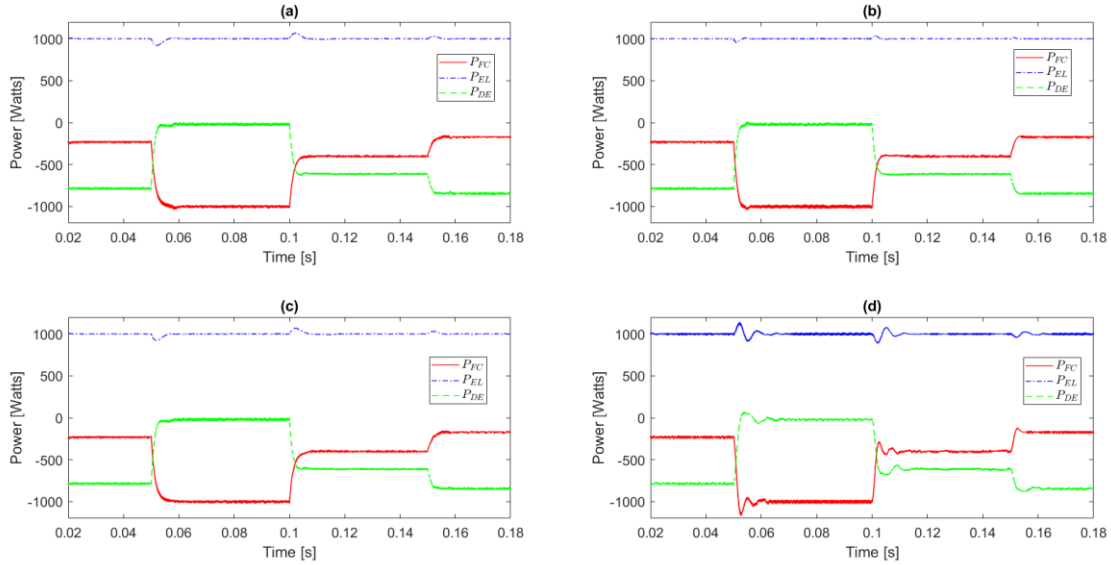


Fig. 13: Power flow plots showing deviations on $P_{el}$ at step changes of $I_{fc}$ at 0.05s, 0.1s and 0.15s. (a) Simplified decoupling method (b) GH decoupling method (c) Inverted decoupling method and (d) Without decoupling method.

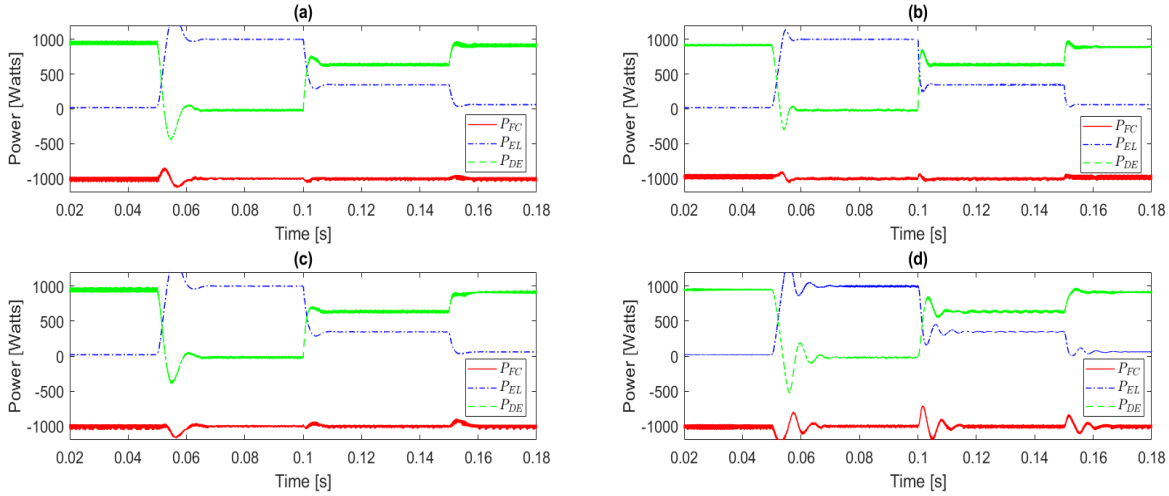


Fig. 14: Power flow plots showing deviations on $P_{fc}$ at step changes of $V_{el}$ at 0.05s, 0.1s and 0.15s. (a) Simplified decoupling method (b) GH decoupling method (c) Inverted decoupling method and (d) Without decoupling method

## V. CONCLUSION

In this paper, a multiport-isolated bidirectional full-bridge DC-DC converter (three port system) for FC and EL applications was presented. This topology aims to limit the bulky conversion stages of the multiple converters used in conventional hydrogen storage systems. This ensures consistent hydrogen production, which can be stored and/or used by the FC to generate electricity. However, the cross-coupling effect in the control loops of the converter has been identified as a major limitation. This makes it difficult to control the converter. The controlled variable in one port affects the other port, leading to a deviation from its steady-state operation and unintended power leakage to the other port. This unintended power flow can cause damage to equipment connected to either port.

This study compared the performance of the converter when a controller with no decoupler and three decoupling controller methods were used to control the TAB in two scenarios. The results showed that the decoupling control enables improved system reliability compared with the converter with no decoupler in the control system. Essentially, with decoupling control, each control loop can act independently. The GH decoupling method provided superior performance in terms of reduced peak power deviation and faster settling time when a step change was applied.

## REFERENCES

[1] P. Breeze, "Hydrogen Energy Storage," in *Power System Energy Storage Technologies*: Elsevier, 2018, pp. 69-77.

[2] M. Yue, H. Lambert, E. Pahon, R. Roche, S. Jemei, and D. Hissel, "Hydrogen energy systems: A critical review of technologies, applications, trends and challenges," in *Renewable and Sustainable Energy Reviews* vol. 146, ed: Elsevier Ltd, 2021.

[3] V. Guida, D. Guilbert, and B. Douine, "Candidate Interleaved DC-DC Buck Converters for Electrolyzers: State-of-the-Art and Perspectives," in *2018 IEEE International Conference on Environment and Electrical Engineering and 2018 IEEE Industrial and Commercial Power Systems Europe (EEEIC / I&CPS Europe)*, 12-15 June 2018 2018, pp. 1-6, doi: 10.1109/EEEIC.2018.8494457.

[4] D. Guilbert, S. M. Collura, and A. Scipioni, "DC/DC converter topologies for electrolyzers: State-of-the-art and remaining key issues,"

in *International Journal of Hydrogen Energy* vol. 42, ed: Elsevier Ltd, 2017, pp. 23966-23985.
[5] D. Guilbert, A. Gaillard, A. Mohammadi, A. N'Diaye, and A. Djerdir, "Investigation of the interactions between proton exchange membrane fuel cell and interleaved DC/DC boost converter in case of power switch faults," *International Journal of Hydrogen Energy*, vol. 40, no. 1, pp. 519-537, 2015, doi: 10.1016/j.ijhydene.2014.10.072.
[6] A. Andrijanovits, "New Converter Topologies for Integration of Hydrogen Based Long-Term Energy Storages to Renewable Energy Systems," PhD., Department of Electrical Engineering, Tallinn University Of Technology, 2013.
[7] A. Andrijanovits, A. Blinov, D. Vinnikov, And J. Martins, "Magnetically Coupled Multiport Converter with Integrated Energy Storage," *PRZEGLĄD ELEKTROTECHNICZNY (Electrical Review),* 2012.
[8] D. Vinnikov, O. Husev, A. Andrijanovits, and I. Roasto, "New High Gain Step Up Dc DC Converter for a Fuel Cell Interfacing in Hydrogen Buffer," 2011.
[9] M. Jafari, Z. Malekjamshidi, G. Platt, and J. G. Zhu, "A Multi-Port Converter Based Renewable Energy System for Residential Consumers of Smart Grid," *IECON2015 Yokohama*, November 9-12 2015.
[10] J. Li, Q. Luo, T. Luo, D. Mou, and M. Liserre, "Efficiency Optimization Scheme for Isolated Triple Active Bridge DC–DC Converter With Full Soft-Switching and Minimized RMS Current," *IEEE Transactions on Power Electronics*, vol. 37, no. 8, pp. 9114-9128, 2022, doi: 10.1109/tpel.2022.3157443.
[11] D. Vinnikov, A. Andrijanovits, I. Roasto, and T. Jalakas, "Experimental Studey of New Intergrated Dc DC Converter for Hydrogen Based Energy Storage," presented at the International Symposium on Power Electronics, Electrical Drives, Automation and Motion, 2011.
[12] Y. A. Harrye, K. H. Ahmed, and A. A. Aboushady, "DC fault isolation study of bidirectional dual active bridge DC/DC converter for DC transmission grid application," *IECON 2015 - 41st Annual Conference of the IEEE Industrial Electronics Society*, pp. 3193-3198, 2015, doi: 10.1109/IECON.2015.7392592.
[13] Y. Cai, C. Gu, J. Li, J. Yang, G. Buticchi, and H. Zhang, "Dynamic Performance Enhancement of a Triple Active Bridge with Power Decoupling-Based Configurable Model Predictive Control," *IEEE Transactions on Transportation Electrification*, pp. 1-1, 2022, doi: 10.1109/tte.2022.3226471.
[14] D. N. Pawar and N. M. Singh, "MPC based Controller for Dual Active Bidirectional DC–DC Converter Driving Inverter using Dynam ic Phasor Approach," presented at the IEEE International Conference on Power, Control, Signals and Instrumentation Engineering, 2017.
[15] O. M. Hebala, "Design and Analysis of Current Stress Minimisation Controllers in Multi Active Bridge DC-DC Converters," ed, 2020.
[16] O. M. Hebala, A. A. Aboushady, K. H. Ahmed, and I. Abdelsalam, "Generalized Active Power Flow Controller for Multiactive Bridge DC–DC Converters With Minimum-Current-Point-Tracking Algorithm," *IEEE Transactions on Industrial Electronics*, vol. 69, no. 4, pp. 3764-3775, 2022, doi: 10.1109/tie.2021.3071681.
[17] R. W. Erickson, ""“Optimal single resistors damping of input filters," presented at the Applied Power Electronics Conference and Exposition, March. 1999.
[18] L. Xing, F. Feng, and J. Sun, "Optimal Damping of EMI Filter Input Impedance," *IEEE Transactions on Industry Applications*, vol. 47, no. 3, pp. 1432–440, March 2011.
[19] A. B. Awan, S. Pierfederici, B. Nahid-Mobarakeh, and Farid, "Active stabilization of a poorly damped input filter supplying a constant power load," presented at the IEEE Energy Conversion Congress and Exposition, Sept 2009.
[20] A. Riccobono and E. Santi, "A novel Passivity-Based Stability Criterion (PBSC) for switching converter DC distribution systems," presented at the Applied Power Electronics Conference and Exposition (APEC) , Twenty-Seventh Annual IEEE, March .2012.
[21] G. Adam, K. Ahmed, N. Singh, S. Finney, And B. Williams, "H-Bridge Modular Multilevel Converter (M2c) For High-Voltage Applications," presented at the 21st International Conference on Electricity Distribution Frankfurt, 6-9 June, 2011
[22] D.-U. Kim, B. J. ByengJoo Byen, and S. Kim, "Design of Triple-Active Bridge Converter with Inherently Decoupled Power Flows," *EPE'22 ECCE Europe*, 2022.
[23] S. Bandyopadhyay, P. Purgat, Z. Qin, and P. Bauer, "A Multiactive Bridge Converter With Inherently Decoupled Power Flows," *IEEE Transactions on Power Electronics*, vol. 36, no. 2, pp. 2231-2245, 2021, doi: 10.1109/tpel.2020.3006266.
[24] P. Purgat, S. Bandyopadhyay, Z. Qin, and P. Bauer, "Power Flow Decoupling Controller for Triple Active Bridge Based on Fourier Decomposition of Transformer Currents," presented at the IEEE, 2020.
[25] S. S. Shah, V. M. Iyer, and S. Bhattacharya, "An approach to unified full-order modeling of dual active bridge type converters," *Proceedings: IECON 2018 - 44th Annual Conference of the IEEE Industrial Electronics Society*, pp. 986-992, 2018, doi: 10.1109/IECON.2018.8591664.
[26] H. Tao, A. Kotsopoulos, J. L. Duarte, and M. A. M. Hendrix, "A Soft-Switched Three-Port Bidirectional Converter for Fuel Cell and Supercapacitor Applications," 2005.
[27] Y. Chen, P. Wang, H. Li, and M. Chen, "Power Flow Control in Multi-Active-Bridge Converters: Theories and Applications," *IEEE Applied Power Electronics Conference and Exposition*, 2019.
[28] K. O. Bempah, K.-W. Heo, and J.-H. Jung, "Power flow decoupling method of triple-active-bridge converter for islanding mode operation in DC microgrid systems," *Journal of Power Electronics*, vol. 23, no. 1, pp. 58-67, 2022, doi: 10.1007/s43236-022-00528-5.
[29] A. Chandwani, A. Mallik, and A. M. Kannan, "A Novel Decoupled Control Scheme for Phase Controlled Triple Active Bridge," presented at the IECON 2021 – 47th Annual Conference of the IEEE Industrial Electronics Society, 2021.
[30] K. Nishimoto, Y. Kado, and K. Wada, "Implementation of Decoupling Power Flow Control System in Triple Active Bridge Converter Rated at 400V, 10kW, and 20kHz," *IEEJ Journal of Industry Applications*, vol. 7, no. 5, pp. 410-415, 2018, doi: 10.1541/ieejjia.7.410.
[31] C. Zhao, S. D. Round, and J. W. Kolar, "An Isolated Three-Port Bidirectional DC-DC Converter With Decoupled Power Flow Management," *IEEE Transactions on Power Electronics*, vol. 23, no. 5, pp. 2443-2453, 2008, doi: 10.1109/tpel.2008.2002056.
[32] R. W. A. A., D. Doncker., Deepakraj M. Divan, and M. H. Kheraluwala, "A Three-phase Soft-Switched High-Power-Density dc /dc Converter for High-Power Applications," *IEEE TRANSACTIONS ON INDUSTRY APPLICATIONS*, vol. 27, no. 1, 1991.
[33] A. G. GANZ, "A Simple, Exact Equivaknt Circuit for the Three - Winding Transformer," *IRE TRANSACTIONS ON COMPONENT PA.RTS*, p. 2, 1962.
[34] T. Hoeksma, "A Dual Active Bridge Based Battery Controller with Zero Voltage Switching for a Grid-Tied Small Wind Turbine," presented at the University of Twente, 2022.
[35] B. Zhao, Q. Song, W. Liu, and Y. Sun, "Overview of dual-active-bridge isolated bidirectional DC-DC converter for high-frequency-link power-conversion system," *IEEE Transactions on Power Electronics*, vol. 29, no. 8, pp. 4091-4106, 2014, doi: 10.1109/TPEL.2013.2289913.
[36] "5.6__Delta-Y_(Pi-T)_Conversions," vol. 2022, ed. https://eng.libretexts.org/@go/page/25270: LibreTexts.
[37] H. Bai and C. Mi, "Eliminate reactive power and increase system efficiency of isolated bidirectional dual-active-bridge dc-dc converters using novel dual-phase-shift control," *IEEE Transactions on Power Electronics*, vol. 23, no. 6, pp. 2905-2914, 2008, doi: 10.1109/TPEL.2008.2005103.
[38] B. Zhao, Q. Song, and W. Liu, "Power characterization of isolated bidirectional dual-active-bridge dc-dc converter with dual-phase-shift control," *IEEE Transactions on Power Electronics*, vol. 27, no. 9, pp. 4172-4176, 2012, doi: 10.1109/TPEL.2012.2189586.
[39] L. Liu, S. Tian, D. Xue, T. Zhang, Y. Chen, and S. Zhang, "A Review of Industrial MIMO Decoupling Control," *International Journal of Control, Automation and Systems*, vol. 17, no. 5, pp. 1246-1254, 2019, doi: 10.1007/s12555-018-0367-4.
[40] H. L. Wade, "Inverted decoupling a neglected technique," *ISA Transactions*, vol. 36, no. 1, pp. 3-10, 1997.
[41] D. Vinnikov, A. Andrijanovitš, I. Roasto, and T. Lehtla, "New integrated converter for hydrogen buffer interfacing in distributed energy systems," *Renewable Energy and Power Quality Journal*, pp. 998-1003, 2011, doi: 10.24084/repqj09.525.